A high-speed automatic spectrometer based on a solid-state non-collinear acousto-optic tunable filter

Jianhua Zhu (朱建华)[1] and Andrew Y. S. Cheng (郑玉臣)[2]

[1] *Information Optics Institute, Sichuan University, Chengdu 610064*

[2] *Department of Physics and Materials Science, City University of Hong Kong, Hong Kong*

Received July 11, 2002

An automatic visible spectrometer based on a non-collinear acousto-optic tunable filter (AOTF) is constructed for high-speed spectrometry. Its spectral filtering characteristics, such as relationships between the radio-frequency (RF) driving frequency and the output central wavelength, the output bandwidth and the central wavelength, its typical spectral point spread function (PSF), and so on, are studied systematically. The preliminary measurement results of AOTF spectrometer show that it is a solid-state, high-speed, easily controllable by computer-programming, rugged and compact spectroscopic device in comparison with a conventional grating spectrometer, and has the potential for widespread spectrometric applications.

OCIS codes: 120.6200, 300.6190, 300.6550, 160.1050.

AOTF is an electronically tunable optical filter based on acousto-optic interaction in an anisotropic medium[1,2]. It consists of a birefringent optical material coupled to a RF acoustic driver (a piezoelectric transducer). Application of a narrow band RF power deflects the selected wavelength interval from the polychromatic beam. The output wavelength is governed by the applied frequency of acoustic wave. Compared with conventional prism and grating spectrometers, AOTF has many excellent characteristics, such as rapid wavelength access, large angular aperture, all solid-state, compactness, ruggedness, *etc*, and is almost an ideal device for visible and near-infrared spectroscopy. In recent years, with the progress in growth methods for acousto-optic crystals and fabricating methods for piezoelectric transducers, commercially available high-quality AOTF has drawn much attention and has been employed for quite a few spectrometric and spectral imaging applications[3−6]. Recently, we presented our research results of AOTF spectrometer in the near-infrared spectral region[7]. In this paper, the spectroscopic characteristics of a TeO_2 AOTF in visible spectral region are studied in detail and an automatic high-speed AOTF spectrometer with moderate spectral resolution is constructed for visible spectrometry. Some characteristic analyses and discussions are also given.

Generally, when an AOTF operates in a non-collinear configuration, the acoustic and optical waves propagate at quite different angles through the crystal. The wavelength of diffracted light is given by the following equation

$$\lambda = \frac{\nu \Delta n}{f} \sqrt{\sin^4 \Theta_i + \sin^2 2\Theta_i}, \tag{1}$$

where ν and f are the velocity and frequency of the employed acoustic wave, Δn is the difference in the refractive indices for the incident and diffracted radiation, Θ_i is the polar angle of the incident light beam and the acoustic wave. Equation (1) shows an inverse proportional relationship between the output central wavelength and the RF driving frequency. Another important parameter is the band-pass of the diffracted light, which depends on the central wavelength of the diffracted light. The full width at half maximum (FWHM), $\Delta\lambda$, is given as

$$\Delta\lambda = \frac{\lambda^2}{2\Delta n L \sin^2 \Theta_i}. \tag{2}$$

All parameters are defined previously except for L, which is the interaction length between the acoustic wave and optical radiation. From Eq. (2), we can find that $\Delta\lambda$ is proportional to the square of the central wavelength, if all other parameters are constant. This relationship means that better resolution will occur at shorter wavelengths.

The systematic investigations of AOTF characteristics are the key issue of constructing a successful spectrometric application. A schematic diagram of the experimental setup for characterization of AOTF is shown in Fig. 1. The tellurium dioxide (TeO_2) non-collinear AOTF used in this study is a product of Brimrose Corp. (Model TEAF 7-.36-.54H) with a spectral range from 350 to 550 nm and a square optical aperture of 7×7 mm^2. The output wavelength is governed by the applied frequency of acoustic wave, which is generated and controlled by a RF synthesizer through a personal computer. A xenon lamp is collimated using a biconcave lens before the AOTF and an optical mask is placed in the optical path after the AOTF to block the zero order and unwanted diffraction order. The filtered narrow-band light is focused and collected by light-guided polymer optic

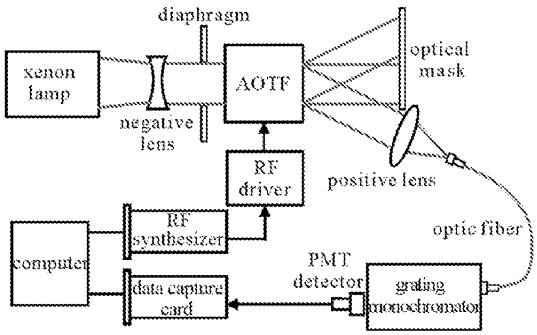

Fig. 1. Experimental setup for the characterization of AOTF.

fiber with a diameter of 2000 μm, and the output light from optic fiber is coupled to a scanning grating monochromator. Then a photomultiplier tube (PMT) detector performs the optic-electric conversion of monochromatic light and transfers the electrical signal to a 16-bit high-speed data capture card for the following data acquisition, storage and analysis of spectral parameters in a Pentium III personal computer. During the characterizing process, experiments were conducted with various minor alterations, detecting scheme and different light sources.

A medium-resolution scanning grating monochromator (Model 7300, Applied PhotoPhysics Limited) was used in our experiments to test the filtering characteristics. Its scanning function will allow for a systematic search for the peak central wavelength at different RF driving frequencies. Because the spectral resolution of the grating spectrometer is set to 0.1 nm, which is much narrower than the spectral band-pass of AOTF, it will not influence the measurements of the AOTF characteristics. With the AOTF tuned to a particular frequency, grating is scanned, and the wavelength at peak detector intensity is recorded. The output central wavelengths versus inverse driving frequencies are plotted in Fig. 2. A good first-order fitting to the data shows an inverse proportional relationship between the output wavelength and the driving frequency. The measurement results have a good agreement with theoretical expression in Eq. (1). A numerical expression was found to feed the programming demand of controlling output wavelengths

$$\lambda(\mathrm{nm}) = 36285/f(\mathrm{MHz}) + 160.5, \tag{3}$$

where λ is the central wavelength of the band-pass in nm, and f is RF driving frequency in megahertz. Although it is not an exact description of the relationship between the driving frequency and the output wavelength, Eq. (3) is very helpful and can be used in the computer programs to control the spectral wavelengths of the AOTF in experiments.

Using the same setup for measuring the peak central wavelength of the AOTF, the spectral point spread function (PSF) of the AOTF can be readily measured. When the AOTF tuned to a particular frequency, grating is scanned to record the filtered narrow-band spectrum from AOTF, i.e., the spectral point spread function. Figure 3 gives a sample PSF spectrum at central wavelength of 381.4 nm, which has a band-width of 1.4 nm. It can be

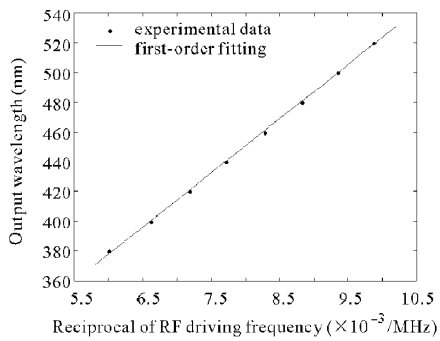

Fig. 2. The output central wavelengths of the AOTF at different RF driving frequencies.

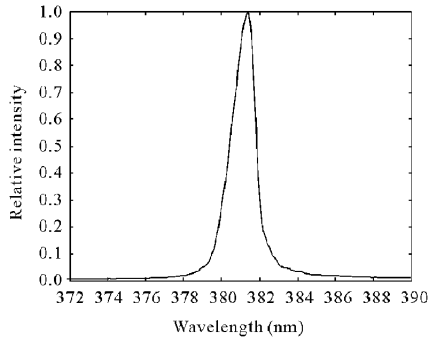

Fig. 3. The typical spectral point spread function of the AOTF.

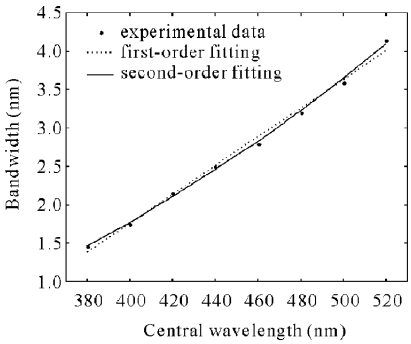

Fig. 4. The spectral bandwidth versus the central wavelength.

observed that the PSF curve has an asymmetric shape. This is somewhat inconsistent with the theory of **K**-vector matching for an ideal AOTF crystal. However, after repeated experiments to eliminate the asymmetry, the asymmetric feature was still present. We think that this may be due to the acoustic inhomogeneities of the particular crystal used in the experiment[7]. From each of the spectral PSF profiles with different band-centered wavelengths, the output bandwidth $\Delta\lambda$ at FWHM and the related central wavelength can be obtained. The experimental result and its first-order and second-order fitting curves to the measurement data are also plotted in Fig. 4. Their numerical expressions are given as

First-order fitting:

$$\Delta\lambda_1(\mathrm{nm}) = 0.0188\lambda(\mathrm{nm}) - 5.7643 \tag{4}$$

Second-order fitting:

$$\Delta\lambda_2(\mathrm{nm}) = 2.9762\mathrm{e} - 5\lambda^2(\mathrm{nm}) - 0.008\lambda(\mathrm{nm}) + 0.2 \tag{5}$$

The root mean square (RMS) errors are 0.072 and 0.042 nm for 1st and 2nd fitting curves, respectively. So the second-order fitting shows a better result than the first-order fitting. This result is in agreement with the theoretical squared relationship between the output bandwidth and the central wavelength in Eq. (2).

Finally, based on the above characterization of AOTF, an automatic AOTF spectrometer is constructed in our laboratory for spectrometric measurements and spectroscopic applications. The schematic layout of our AOTF

spectrometer is shown in Fig. 5. Unlike the experimental setup for the research of AOTF characteristics, an optical chopper is employed in the AOTF spectrometer to modulate the continuous radiation from light source into an alternate radiation. This will eliminate the accumulated thermal noise and radiation damage of PMT detector. When the reference modulation signal from the optical chopper is transferred to the lock-in amplifier (Model SR830, Stanford Research System Inc.), the phase sensitive characteristic of the lock-in amplifier will enable the high-stability signal acquisition of PMT detector. Then the 16-bit high-speed data capture card performs the high-precision spectral data capture, storage, and analysis.

After the AOTF spectrometer is constructed, its frequency jitter and stability testing are conducted. As mercury lamp has some characteristic spectral lines in the spectral region of our AOTF spectrometer, we use mercury lamp as light source to carry out the performance test. After repeated spectral measurements of mercury lamp, no obvious peak wavelength shifts are observed during the whole testing procedures. Meanwhile, the peak intensities of its spectral lines keep much stable, their variations are below 0.5%, which shows a high stability and repeatability of the AOTF spectrometer. Figures 6 and 7 are the spectra of mercury lamp and fluorescent energy-saving lamp measured by the AOTF spectrometer. The characteristic spectral lines of mercury radiation at 365.0, 404.6 and 435.8 nm can be clearly resolved in Fig. 6. By comparing Fig. 7 with Fig. 6, we

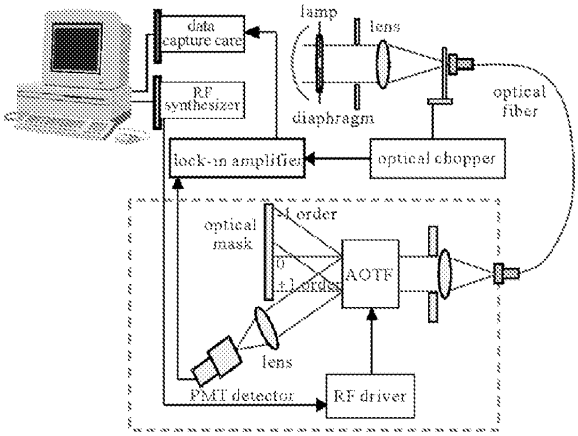

Fig. 5. The schematic layout of AOTF spectrometer.

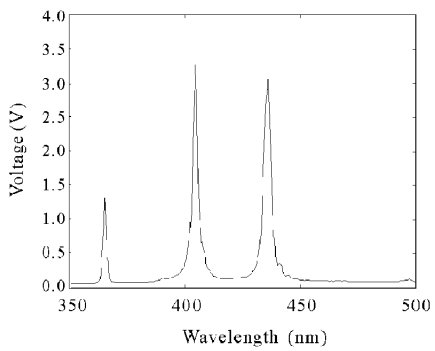

Fig. 6. Measured spectrum of mercury lamp using AOTF spectrometer.

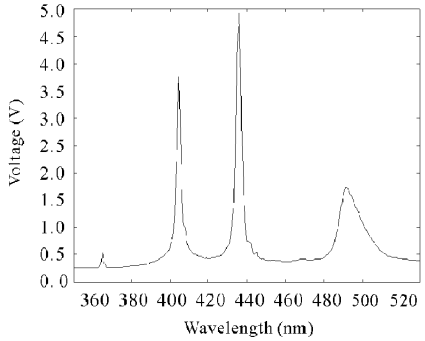

Fig. 7. Measured spectrum of fluorescent energy-saving lamp using AOTF spectrometer.

can find that there is a wide spectral band around 490 nm in Fig. 7 besides the intensity variations of characteristic mercury lines. The measurement process can be conducted at very short time, typically several seconds (the measurement time of grating spectrometer over a long spectral range is typically from several minutes to several tens of minutes). Besides, the measured spectra in our experiments also have reasonable agreements with other reference spectra of these light sources, which shows that our AOTF spectrometer is a high-speed spectrometer with medium resolution and can be readily used for the spectral measurements and spectroscopic applications without causing significant deviations.

In conclusion, AOTF is a solid-state, high-speed, rugged and compact spectroscopic device and has potential applications in real-time spectral measurement, online process monitoring, color-imaging, *etc.* The filtering characteristics of the noncollinear TeO_2 AOTF used in the visible light region are studied systematically in this paper. By changing the frequency of the acoustic wave, one can rapidly vary the diffracted light wavelength at a microsecond time scale. The output central wavelength exhibits an inverse proportional relation with the RF driving frequency, and the spectral bandwidth shows a square relation with the central wavelength. Our AOTF spectrometer has a spectral resolution of 1.75 nm at 400 nm, and can be satisfactory for many spectroscopic measurements and applications without significant deviation.

This work was supported by the National Natural Sciences Foundation of China under Grant No. 60007002.
J. Zhu's e-mail address is zhujh123@hotmail.com.

References

1. I. C. Chang, Proc. SPIE **90,** 12 (1976).
2. C. D. Tran, Anal. Chem. **64,** 971A (1992).
3. C. D. Tran, R. J. Furlan, and J. Lu, Appl. Spectrosc. **48,** 101 (1994).
4. C. D. Tran and R. J. Furlan, Anal. Chem. **64,** 2775 (1992).
5. D. P. Baldwin, D. S. Zamzow, and A. P. D'Silva, Appl. Spectrosc. **50,** 498 (1996).
6. D. R. Suhre, M. Gottlieb, L. H. Taylor, and N. T. Melamed, Opt. Eng. **31,** 2118 (1992).
7. A. Y. S. Cheng, J. H. Zhu, and M. C. Y. Pau, Appl. Spectrosc. **55,** 350 (2001).